Editors' Suggestion

Joint Cosmic Microwave Background and Big Bang Nucleosynthesis Constraints on Light Dark Sectors with Dark Radiation

Cara Giovanetti,[1,*] Mariangela Lisanti,[2,3,†] Hongwan Liu,[1,2,‡] and Joshua T. Ruderman[1,§]
[1]*Center for Cosmology and Particle Physics, Department of Physics, New York University, New York, New York 10003, USA*
[2]*Department of Physics, Princeton University, Princeton, New Jersey 08544, USA*
[3]*Center for Computational Astrophysics, Flatiron Institute, 162 Fifth Ave, New York, New York 10010, USA*

(Received 17 September 2021; revised 8 March 2022; accepted 3 June 2022; published 6 July 2022)

Dark sectors provide a compelling theoretical framework for thermally producing sub-GeV dark matter, and motivate an expansive new accelerator and direct-detection experimental program. We demonstrate the power of constraining such dark sectors using the measured effective number of neutrino species, N_{eff}, from the cosmic microwave background (CMB) and primordial elemental abundances from big bang nucleosynthesis. As a concrete example, we consider a dark matter particle of arbitrary spin that interacts with the standard model via a massive dark photon, accounting for an arbitrary number of light degrees of freedom in the dark sector. We exclude dark matter masses below $\sim$4 MeV at 95% confidence for all dark matter spins and dark photon masses. These bounds hold regardless of additional new light, inert degrees of freedom in the dark sector, and for dark matter-electron scattering cross sections many orders of magnitude below current experimental constraints. The strength of these constraints will only continue to improve with future CMB experiments.

DOI: 10.1103/PhysRevLett.129.021302

Introduction.—The exquisite precision of the cosmic microwave background (CMB) and big bang nucleosynthesis (BBN) measurements has historically played an important role in constraining the properties of dark matter (DM) [1–15]. The introduction of new particles in the dark sector can affect the expansion rate of the Universe, as well as the temperature of standard model (SM) particles, thereby leaving distinctive signatures on both elemental abundances and the effective number of neutrino species, N_{eff}. In this Letter, we demonstrate how to compute joint CMB and BBN constraints for generic dark sectors, using the example of a sub-GeV DM species accompanied by a massive dark photon and an arbitrary number of light, inert degrees of freedom.

Joint CMB and BBN constraints have been obtained for a single DM particle in thermal equilibrium with the SM at early times [7–10,13–17]. For example, Refs. [14,15] find that an electromagnetically coupled DM particle must have mass $m_\chi \gtrsim 5$ MeV at 95% confidence, depending on its spin. However, the need for joint constraints is more significant for dark sectors. This was underscored by Refs. [8,11,17], which obtained joint CMB and BBN constraints for electromagnetically coupled DM accompanied by additional relativistic degrees of freedom in the dark sector. In this model, CMB-only constraints cannot break the degeneracy between DM entropy injection—which heats photons relative to neutrinos after neutrino decoupling, leading to a lower value of N_{eff}—and new inert, relativistic degrees of freedom. Primordial elemental abundances are affected in different ways by the radiation energy density and the neutrino temperature during BBN, and can therefore break this degeneracy.

Beyond these simple models, CMB and BBN constraints have the potential to play an important role in our understanding of well-motivated dark sectors, many of which yield viable thermal relics in the keV–GeV mass range (see, e.g., Refs. [18–36]). These dark sectors commonly have multiple states that interact with the SM through portal interactions, which need to be properly accounted for when determining the joint CMB and BBN constraints. Furthermore, new numerical methods [37,38] now allow for such joint constraints to be calculated with the inclusion of many potentially important effects, including noninstantaneous neutrino decoupling and BBN nuclear rate uncertainties.

We focus on a scenario where the DM particle χ couples to a massive U(1)' dark photon A' that is kinetically mixed with the SM photon. We also include the possibility of new inert, relativistic degrees of freedom, which has been used to avoid CMB-only N_{eff} constraints due to the aforementioned degeneracy with DM entropy injection (see, e.g., Refs. [7,10,39–41]). This model is one of the standard benchmarks for the nascent experimental program for the direct detection of DM-electron scattering [42].

Using the 2018 Planck results [43], as well as the primordial elemental abundances from Refs. [44,45], we robustly constrain the DM mass m_χ as a function of its spin and the dark photon mass $m_{A'}$. For example, when $m_{A'}/m_\chi = 3$, we exclude complex scalar (Dirac fermion) DM below $m_\chi \sim 5.2$ MeV (7.9 MeV) at 95% confidence for DM-electron scattering cross sections that are many orders of magnitude below current constraints. These results apply regardless of the number of inert, relativistic degrees of freedom in the model, thereby circumventing a key weakness of previous cosmological constraints of this kind. They will also strengthen with future CMB measurements.

Methodology.—We compute the effect of a dark sector model with parameters $\boldsymbol{\theta}$ on the effective number of relativistic degrees of freedom at late times, $N_{\rm eff}$. For our benchmark model,

$$N_{\rm eff} = 3\left[\frac{11}{4}\left(\frac{T_\nu}{T_\gamma}\right)^3_0\right]^{4/3}\left(1+\frac{\Delta N_\nu}{3}\right). \qquad (1)$$

Here, T_γ and T_ν are the photon and neutrino temperatures, respectively, and ΔN_ν is the ratio of the energy density ρ_ξ of inert, relativistic degrees of freedom ξ in the dark sector to that of a single neutrino at late times, taking $\rho_\xi \propto a^{-4}$ throughout cosmic history. The benchmark model consists of two free parameters, m_χ and ΔN_ν; $m_{A'}$ is set as a constant multiple of m_χ. The subscript "0" denotes a late point in time when $T_\gamma \ll m_\chi$, $m_{A'}$, and m_e, the electron mass. As demonstrated by Eq. (1), annihilations that preferentially inject entropy into the photon bath decrease $N_{\rm eff}$ relative to the standard cosmological value. This decrease, which depends on m_χ, can be compensated for by increasing ΔN_ν. Appendix A in the Supplemental Material reviews how dark sectors impact T_γ and T_ν [46].

We also determine the effect of the dark sector on the primordial abundances of elements after BBN has ended. We only consider Y_P and D/H, the ratio of the abundance by mass of helium-4 and the ratio of the abundance of deuterium to hydrogen, respectively; extending the analysis to other elements is straightforward. We compute Y_P and D/H for a given dark sector model over the range $\Omega_b h^2 \in [0.0218, 0.0226]$—much broader than the Planck uncertainty on this parameter [43]—since the production of light elements is highly sensitive to the baryon-to-photon ratio [8].

These calculations were performed using the public codes nudec_BSM [12,37] and PRIMAT (we use the latest version of PRIMAT [53], which includes the recently updated measurement of the $\mathrm{D}+p \to {}^3\mathrm{He}+\gamma$ cross section [54]) [38,53], which we modify to include a DM particle (of arbitrary spin), a dark photon, and ΔN_ν. Our modified nudec_BSM first computes T_γ and T_ν, as well as the Hubble rate and scale factor as functions of time, self-consistently including the effects of noninstantaneous neutrino decoupling and QED corrections [12,37]. The nudec_BSM output is then used by our modified version of PRIMAT to obtain an accurate prediction of the elemental abundances. This method can be easily extended to any arbitrary dark sector.

To assess the consistency of the computed $N_{\rm eff}(\boldsymbol{\theta})$, $Y_P(\boldsymbol{\theta}, \Omega_b h^2)$, and $\mathrm{D/H}(\boldsymbol{\theta}, \Omega_b h^2)$ with CMB and BBN measurements, we perform a hypothesis test on our model parameters by constructing a profile likelihood ratio. Explicitly, we define

$$L(\boldsymbol{\theta}, \Omega_b h^2) = L_{\rm BBN}(\boldsymbol{\theta}, \Omega_b h^2)\, L_{\rm CMB}(\boldsymbol{\theta}, \Omega_b h^2), \qquad (2)$$

where L is the Gaussian likelihood of the parameters $\boldsymbol{\theta}$ and $\Omega_b h^2$. The contribution from the CMB measurements, $L_{\rm CMB}$, is computed using the central values and covariance matrix from Planck for a fit with the six ΛCDM parameters, plus $N_{\rm eff}$ and Y_P [43,55], with

$$N_{\rm eff} = 2.926 \pm 0.286. \qquad (3)$$

For comparison, we also show projected results for the upcoming Simons Observatory [56].

The contribution from BBN, $L_{\rm BBN}$, is computed using the central values of the observed elemental abundances, and a covariance matrix that combines experimental and theoretical uncertainties. The measured values and uncertainties of Y_P [44] and D/H [45] are

$$Y_P = 0.245 \pm 0.003,$$
$$\mathrm{D/H} = (2.527 \pm 0.030) \times 10^{-5}. \qquad (4)$$

Theoretical uncertainties and correlations between predicted Y_P and D/H values arise from uncertainties in nuclear rates. The D/H theoretical uncertainty varies with both $\boldsymbol{\theta}$ and $\Omega_b h^2$, and can be comparable to or even exceed the measurement uncertainty; it is therefore evaluated at each parameter point. We compute the theoretical uncertainty and correlations of both D/H and Y_P by varying the nuclear rates by 1σ, and adding the resulting fractional variations to the abundances in quadrature. Finally, both theoretical and measurement uncertainties are added in quadrature to obtain the full BBN covariance matrix. Further details on this procedure are provided in Appendix B of the Supplemental Material [46].

We then calculate the profile likelihood ratio $\lambda_p(\boldsymbol{\theta}) = L_p(\boldsymbol{\theta})/\hat{L}_p$, where $L_p(\boldsymbol{\theta}) = \max_{\Omega_b h^2} L(\boldsymbol{\theta}, \Omega_b h^2)$ and $\hat{L}_p = \max_{\boldsymbol{\theta}, \Omega_b h^2} L(\boldsymbol{\theta}, \Omega_b h^2)$. By Wilk's theorem, the quantity $-2\log\lambda_p(\boldsymbol{\theta})$ follows a chi-squared distribution with degrees of freedom given by the number of model parameters [44]. Sixty-eight (ninety-five) percent confidence limits for $\boldsymbol{\theta}$ in our two-parameter benchmark model are therefore set when $-2\log\lambda_p(\boldsymbol{\theta}) = 2.30(6.18)$.

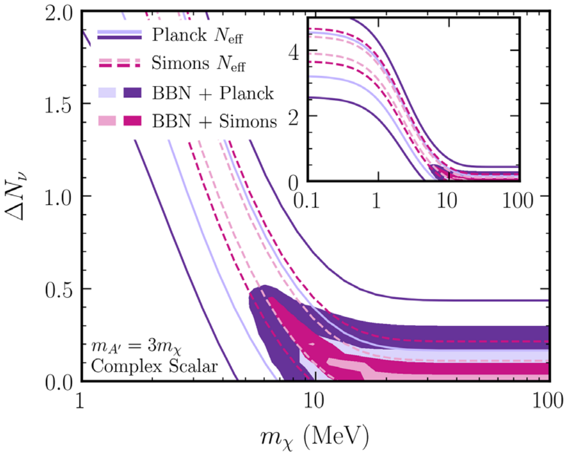

FIG. 1. The allowed region of dark matter mass m_χ and ΔN_ν, for a complex scalar particle and a dark photon with mass $3m_\chi$. The inset shows the same contours over a larger range of m_χ and ΔN_ν. The purple (pink) lines denote the Planck (projected Simons Observatory) $N_{\rm eff}$ 68/95% confidence regions. The corresponding shaded regions correspond to the bounds including BBN measurements. The BBN measurements clearly play a powerful role in setting the lower limit on the dark matter mass, even when $\Delta N_\nu > 0$ is allowed. The value of $\Omega_b h^2$ that maximizes the likelihood was chosen for each parameter point.

Dark photon model constraints.—Figure 1 illustrates the interplay between CMB and BBN measurements in constraining a complex scalar χ and a dark photon with $m_{A'} = 3m_\chi$. The purple (pink) lines correspond to the constraints on m_χ and ΔN_ν that are consistent with the Planck (projected Simons Observatory) measurements. Above $m_\chi \sim 20$ MeV, the predicted value of $N_{\rm eff}$ approaches the standard cosmological value because the DM freezes out well before neutrino decoupling, and so the DM annihilations heat the electromagnetic and neutrino sectors equally.

The impact of the dark sector becomes apparent when $m_\chi \lesssim 20$ MeV, and entropy is injected into the electromagnetic sector during and after the period of neutrino decoupling, when the SM bath has a temperature of $T_{\nu d} \sim 2$ MeV. In this case, $N_{\rm eff}$ decreases relative to the standard value because the electromagnetic sector is preferentially heated, but the photon temperature today is fixed at its measured value of 2.7 K. A nonzero ΔN_ν can restore $N_{\rm eff}$ to its measured value; when m_χ falls below $\sim$20 MeV, the fit clearly prefers a larger ΔN_ν to explain the observed value of $N_{\rm eff}$. Below $m_\chi \lesssim 1$ MeV, the DM is relativistic throughout neutrino decoupling; entropy is dumped only into the electromagnetic sector regardless of mass, and the constraints level off (Fig. 1 inset).

The result of including BBN constraints from Y_P and D/H is indicated by the shaded regions in Fig. 1. BBN clearly adds significant discriminating power, placing a 95% lower confidence bound on the DM mass of $m_\chi \sim 5$ MeV when combined with Planck data, regardless of ΔN_ν. The Simons Observatory will have improved sensitivity to m_χ with its more precise measurement of $N_{\rm eff}$, while also reducing the uncertainty on ΔN_ν.

The introduction of an MeV-scale DM particle and dark photon leads to a variety of effects on BBN physics, which are summarized in Fig. 2 for fixed $\Omega_b h^2 = 0.022358$. The solid (dashed) colored lines correspond to different ratios of $m_{A'}/m_\chi$ for $\Delta N_\nu = 0$ (1). The case where $m_{A'}/m_\chi \to \infty$ is consistent with Refs. [1,3,7,8]. The interplay of the following four quantities is relevant for understanding this behavior: (i) the neutron-proton ratio, which is positively correlated with the helium-4 abundance, (ii) the baryon-to-photon ratio η, which is inversely correlated with the deuterium abundance, (iii) the expansion rate, which impacts both the neutron abundance and the deuterium burning rate [57], and (iv) the rate of neutron-proton interconversion, affected by a modified T_ν (at fixed T_γ). When $m_\chi \gtrsim 3T_{\nu d}$, BBN proceeds as per the standard scenario. When $m_e \lesssim m_\chi \lesssim 3T_{\nu d}$, DM injects significant entropy into the electromagnetic sector after neutrino decoupling. The expansion rate is therefore slower at fixed photon temperature, which drives down the deuterium abundance as there is more time to convert deuterium to heavier elements. Meanwhile, near-cancellation of effects on neutron-proton interconversion and on the expansion rate keeps Y_P essentially constant in this regime [8]. When $m_\chi \lesssim m_e$, the DM acts as a new relativistic species during BBN. This increases the expansion rate, causing weak interactions to decouple earlier, thereby increasing Y_P. In contrast, D/H is further reduced because post-BBN DM annihilations lead to an increased η during BBN

$\Delta N_\nu > 0$ compounds the effect of introducing an MeV-scale DM particle by further increasing the expansion rate. This increases the production of helium-4 and mitigates the decrease in the deuterium abundance. As a result, an increase in ΔN_ν shifts the $\Delta N_\nu = 0$ curves in Fig. 2 upward.

As $m_{A'}/m_\chi$ is reduced, the effects described above are only further enhanced because of the additional entropy injection from the dark photon. In particular circumstances, the presence of the dark photon can qualitatively affect the shape of the D/H and Y_P curves in Fig. 2. For example, the $m_{A'}/m_\chi = 10$ curve exhibits distinctive behavior when $m_\chi \lesssim m_e$. The observed plateau in D/H corresponds to the transition from the point where the dark photon entropy injection heats the photon bath, to the point where the dark photon acts as an additional relativistic species throughout BBN. Elsewhere, the curves for different values of $m_{A'}/m_\chi$ look similar, but the curves shift to the right as $m_{A'}/m_\chi$ decreases, since the entropy injection from the dark photon increases as $m_{A'}$ decreases.

The current measurements of D/H and Y_P are indicated in Fig. 2. For the case where $m_\chi \to \infty$, we find a $\sim$2σ

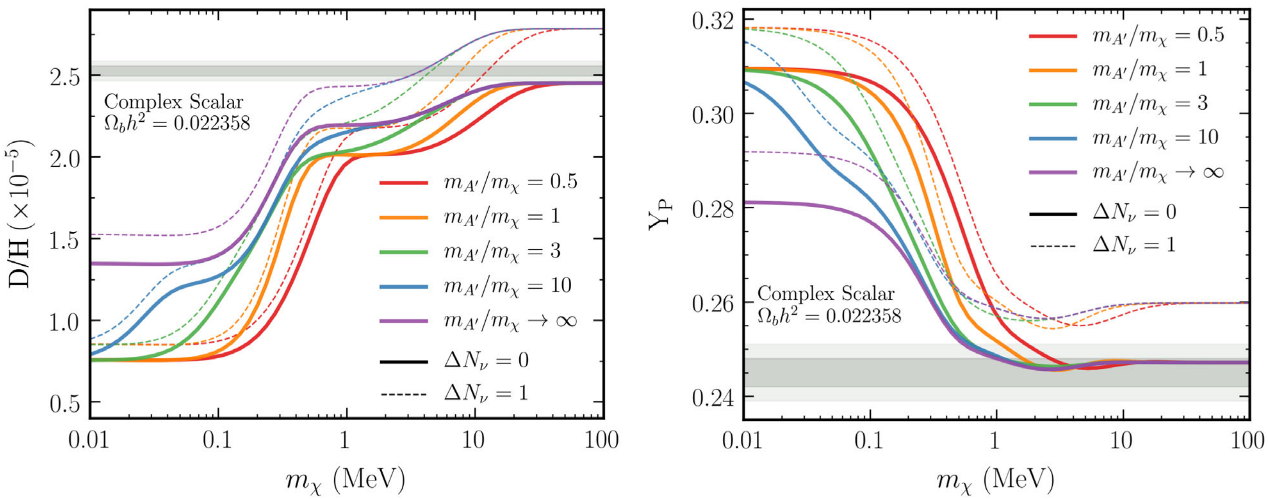

FIG. 2. Predictions for D/H (left) and Y_P (right) for a complex scalar particle χ of mass m_χ. The solid (dashed) lines correspond to $\Delta N_\nu = 0(1)$. The results are shown for five different ratios of dark photon to DM mass: $m_{A'}/m_\chi = 0.5$, 1, 3, 10, and approaching ∞ in red, orange, green, blue, and purple, respectively. The 1 and 2σ uncertainties on the measured values of D/H [45] and Y_P [44] are indicated by the gray horizontal bands. The standard cosmology predictions for D/H and Y_P are consistent with the results in Ref. [53]. $\Omega_b h^2$ is fixed to 0.022358.

discrepancy with the measured deuterium abundance from Ref. [45], consistent with other studies using PRIMAT. References [58,59], which perform independent analyses with different code packages, find better agreement with larger uncertainties. These differences are likely due, at least in part, to differing treatments of the $2\mathrm{D} \to {}^3\mathrm{He} + n$ and $2\mathrm{D} \to {}^3\mathrm{H} + p$ reactions [53,59]. The method presented in this Letter can be easily adapted to account for future improvements in BBN calculations.

Table I enumerates the 95% confidence lower bound on m_χ for a complex scalar, a Majorana fermion, and a Dirac fermion for different values of $m_{A'}/m_\chi$. In all cases, the minimum mass is constant for $m_{A'}/m_\chi \gtrsim 10$ and is a factor of 1.3–1.8 weaker than joint CMB and BBN limits assuming $\Delta N_\nu = 0$ [15]. We find a robust lower bound

TABLE I. The joint Planck CMB and BBN 95% lower limit on the mass of a DM particle that is a complex scalar, Majorana fermion, or Dirac fermion in our benchmark model. The mass limits are provided for different ratios of the dark photon to DM mass. The values in parentheses are the projected Simons Observatory and BBN constraints [14,56]. The value of $\Omega_b h^2$ that maximizes the likelihood was chosen for each parameter point.

	Minimum m_χ (MeV)		
$m_{A'}/m_\chi$	Complex Scalar	Majorana Fermion	Dirac Fermion
0.5	14.3 (16.5)	14.3 (16.5)	15.2 (17.1)
1	9.0 (10.1)	9.0 (10.1)	10.4 (11.5)
1.5	7.1 (8.1)	7.1 (8.0)	9.0 (10.0)
3	5.2 (6.2)	5.0 (6.1)	7.9 (9.1)
≥ 10	4.3 (5.8)	4.0 (5.6)	7.8 (9.1)

of $m_\chi > 3.9$ MeV across all DM particle types, for any nonzero ΔN_ν, using Planck data [43]. The Simons Observatory will be sensitive to heavier masses by several MeV.

The lower bound on m_χ has important implications for experiments searching for dark sector DM. Our benchmark model is commonly used to present bounds and sensitivity projections for direct-detection and accelerator-based experiments. To date, the generality of CMB N_{eff} limits on this model has been questioned due to the degeneracy between DM entropy injection and ΔN_ν [7,10,39–41]. Because our joint CMB and BBN constraints apply for any $\Delta N_\nu > 0$, they address these prior concerns and establish a robust cosmological bound on the dark sector model under consideration.

We present our results in Fig. 3 for $m_{A'} = 3m_\chi$ in terms of the reference DM-electron scattering cross section, $\bar{\sigma}_e \equiv 16\pi\alpha\alpha_D\epsilon^2\mu_{\chi e}^2/(\alpha^2 m_e^2 + m_{A'}^2)^2$, where α, α_D are the electromagnetic and dark sector fine structure constants respectively, ϵ is the SM-A' mixing parameter, and $\mu_{\chi e}$ is the electron-χ reduced mass. We show the lower limit on m_χ for a Dirac fermion and a complex scalar, together with existing direct-detection [60–65] and accelerator [66–71] limits on $\bar{\sigma}_e$, assuming χ makes up all of the DM for direct-detection experiments, and choosing $\alpha_D = 0.5$ for beam experiments. We solve the Boltzmann equation for χ with the processes $\chi\bar{\chi} \leftrightarrow e^+e^-$ and $\mu^+\mu^-$ to obtain (i) $\bar{\sigma}_e$ as a function of m_χ for a symmetric complex scalar χ undergoing a standard freeze-out through annihilation into SM fermions and (ii) the lower limit on $\bar{\sigma}_e$ as a function of m_χ for an asymmetric Dirac fermion χ freezing out through annihilation into SM fermions, given the Planck limits on

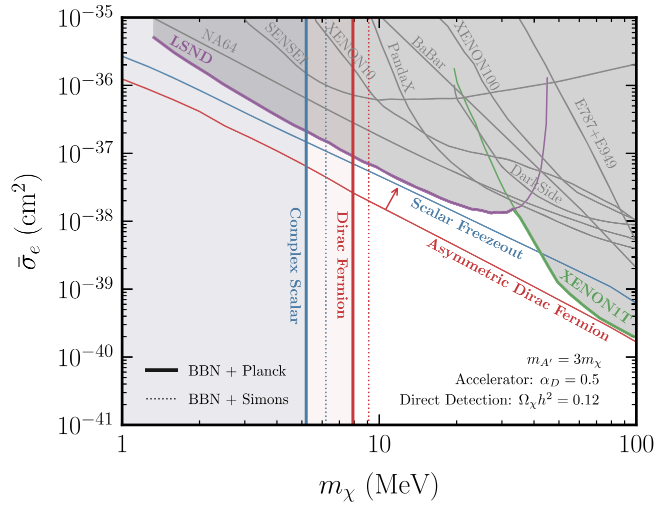

FIG. 3. Joint CMB and BBN 95% confidence constraints on m_χ when χ is a Dirac fermion (shaded red) or a complex scalar (shaded blue), with $m_{A'} = 3m_\chi$. The y axis shows the reference dark matter-electron scattering cross section $\bar{\sigma}_e$. Projected constraints from the Simons Observatory are demarcated by the vertical dotted lines. The blue line indicates where a complex scalar χ undergoes a standard freeze-out to attain the correct relic abundance; the line above which the freeze-out of an asymmetric Dirac fermion χ can produce all of DM is indicated in red. The region of parameter space that is ruled out by experiments at the 90% confidence level is shaded gray, with the strongest constraints coming from Liquid Scintillator Neutrino Detector (LSND) [68] (purple) and XENON1T [63] (green). Other experimental limits are shown as labeled gray lines [60–62,64–67,70,71]. All direct-detection limits on $\bar{\sigma}_e$ assume χ is all of the DM, while accelerator-based limits are independent of the χ abundance, but assume $\alpha_D = 0.5$.

DM annihilation [43,72,73] (see, e.g., Refs. [41,74,75] for similar relic abundance calculations). The joint constraints set a lower limit of $m_\chi > 5.2$ MeV (7.9 MeV) for a complex scalar (Dirac fermion) χ with an arbitrary number of light degrees of freedom at 95% confidence. The Simons Observatory [14,56] is forecasted to have slightly improved sensitivity.

Our limits apply only for dark sectors in chemical equilibrium with the SM while A' is relativistic, where our entropy injection calculation is valid. In the early Universe, processes such as $\chi\bar{\chi} \leftrightarrow e^+e^-$ bring the dark sector into chemical equilibrium with the SM while $T_\gamma \gtrsim m_{A'}$ for sufficiently large $\bar{\sigma}_e$. We estimate this $\bar{\sigma}_e$ by requiring the rate of $e^+e^- \to \chi\bar{\chi}$ to exceed the Hubble rate at $T_\gamma = m_{A'}$, and find $\bar{\sigma}_e \gtrsim 10^{-46}$ cm$^2(10\ \mathrm{MeV}/m_\chi)^3$.

Conclusions.—We have developed a method for obtaining joint CMB and BBN constraints on general dark sectors. As a concrete example, we focused on the dark sector model where a DM particle interacts with the SM through a massive dark photon mediator, including the possibility of an arbitrary number of light degrees of freedom. We place a 95% confidence lower bound of $m_\chi \gtrsim 4$ MeV on the DM mass as long as the dark sector is fully thermalized with the SM in the early Universe. In Table I, we also illustrate how the constraints strengthen with decreasing dark photon mass. Recent studies have identified cosmological and astrophysical probes of $\chi e \to \chi e$ scattering [76,77], resulting in constraints on $\bar{\sigma}_e$ that are many orders of magnitude weaker than the range plotted in Fig. 3 (e.g., $\bar{\sigma}_e \gtrsim 10^{-30}$ cm^2 for $m_\chi = 1$ MeV). Thus, for the example of $m_\chi = 1$ MeV, our constraints are expected to apply between 10^{-43} cm$^2 \lesssim \bar{\sigma}_e \lesssim 10^{-30}$ cm^2, above which $\chi e \to \chi e$ becomes important. To our knowledge, there are no existing models of electrophilic DM that completely evade our bounds, though model-building extensions have been proposed for other scenarios that can weaken the CMB N_{eff} constraints and allow for 1–10 MeV electromagnetically coupled dark sector particles, e.g., by allowing some DM annihilation into neutrinos [12,14,78]. We hope to better understand the robustness of these cosmological limits on generic dark sectors in future work.

Appendices C and D in the Supplemental Material [46] describe the modifications made to nudec_BSM and PRIMAT to handle the dark sector model studied in this Letter. The modified code is available upon request from the authors.

The authors thank Kaustubh Agashe, Alexandre Arbey, Asher Berlin, Kimberly Boddy, Manuel Buen-Abad, Bhaskar Dutta, Rouven Essig, Jonathan Feng, Vera Gluscevic, David McKeen, Siddharth Mishra-Sharma, Cyril Pitrou, Maxim Pospelov, Jordan Smolinsky, Yuhsin Tsai, Neal Weiner, Tien-Tien Yu, and Yiming Zhong for fruitful conversations. This material is based upon work supported by the NSF Graduate Research Fellowship under Grant No. DGE1839302. H. L. and M. L. are supported by the DOE under Award No. DE-SC0007968. M. L. is also supported by the Cottrell Scholar Program through the Research Corporation for Science Advancement. H. L. is also supported by NSF Grant No. PHY-1915409, and the Simons Foundation. J. T. R. is supported by NSF CAREER Grant No. PHY-1554858 and NSF Grant No. PHY-1915409. This work was performed in part at the Aspen Center for Physics, which is supported by NSF Grant No. PHY-1607611. The work presented in this paper was performed on computational resources managed and supported by Princeton Research Computing. This research made extensive use of the publicly available codes nudec_BSM [12,37] and PRIMAT [38,53], as well as the IPYTHON [79], JUPYTER [80], MATPLOTLIB [81], NUMPY [82], and SCIPY [83] software packages.

*cg3566@nyu.edu
†mlisanti@princeton.edu
‡hongwanl@princeton.edu
§ruderman@nyu.edu

[1] Edward W. Kolb, Michael S. Turner, and Terrence P. Walker, Effect of interacting particles on primordial nucleosynthesis, Phys. Rev. D 34, 2197 (1986).

[2] Subir Sarkar, Big bang nucleosynthesis and physics beyond the standard model, Rep. Prog. Phys. **59**, 1493 (1996).
[3] Pasquale Dario Serpico and Georg G. Raffelt, MeV-mass dark matter and primordial nucleosynthesis, Phys. Rev. D **70**, 043526 (2004).
[4] Fabio Iocco, Gianpiero Mangano, Gennaro Miele, Ofelia Pisanti, and Pasquale D. Serpico, Primordial Nucleosynthesis: from precision cosmology to fundamental physics, Phys. Rep. **472**, 1 (2009).
[5] Maxim Pospelov and Josef Pradler, Big bang nucleosynthesis as a probe of new physics, Annu. Rev. Nucl. Part. Sci. **60**, 539 (2010).
[6] Chiu Man Ho and Robert J. Scherrer, Limits on MeV dark matter from the effective number of neutrinos, Phys. Rev. D **87**, 023505 (2013).
[7] Céline Boehm, Matthew J. Dolan, and Christopher McCabe, A lower bound on the mass of cold thermal dark matter from Planck, J. Cosmol. Astropart. Phys. 08 (2013) 041.
[8] Kenneth M. Nollett and Gary Steigman, BBN and the CMB constrain light, electromagnetically coupled WIMPs, Phys. Rev. D **89**, 083508 (2014).
[9] Kenneth M. Nollett and Gary Steigman, BBN and the CMB constrain neutrino coupled light WIMPs, Phys. Rev. D **91**, 083505 (2015).
[10] Ryan J. Wilkinson, Aaron C. Vincent, Céline Bœhm, and Christopher McCabe, Ruling out the light weakly interacting massive particle explanation of the Galactic 511 keV line, Phys. Rev. D **94**, 103525 (2016).
[11] Daniel Green and Surjeet Rajendran, The cosmology of Sub-MeV dark matter, J. High Energy Phys. 10 (2017) 013.
[12] Miguel Escudero, Neutrino decoupling beyond the Standard Model: CMB constraints on the Dark Matter mass with a fast and precise Neff evaluation, J. Cosmol. Astropart. Phys. 02 (2019) 007.
[13] Paul Frederik Depta, Marco Hufnagel, Kai Schmidt-Hoberg, and Sebastian Wild, BBN constraints on the annihilation of MeV-scale dark matter, J. Cosmol. Astropart. Phys. 04 (2019) 029.
[14] Nashwan Sabti, James Alvey, Miguel Escudero, Malcolm Fairbairn, and Diego Blas, Refined bounds on MeV-scale thermal dark sectors from BBN and the CMB, J. Cosmol. Astropart. Phys. 01 (2020) 004.
[15] Nashwan Sabti, James Alvey, Miguel Escudero, Malcolm Fairbairn, and Diego Blas, Implications of LUNA for BBN and CMB constraints on MeV-scale thermal dark sectors, J. Cosmol. Astropart. Phys. 08 (2021) A01.
[16] Céline Boehm, Matthew J. Dolan, and Christopher McCabe, Increasing Neff with particles in thermal equilibrium with neutrinos, J. Cosmol. Astropart. Phys. 12 (2012) 027.
[17] Gary Steigman, Equivalent neutrinos, light WIMPs, and the chimera of dark radiation, Phys. Rev. D **87**, 103517 (2013).
[18] C. Boehm and Pierre Fayet, Scalar dark matter candidates, Nucl. Phys. **B683**, 219 (2004).
[19] Maxim Pospelov, Adam Ritz, and Mikhail B. Voloshin, Secluded WIMP dark matter, Phys. Lett. B **662**, 53 (2008).
[20] Jonathan L. Feng and Jason Kumar, The WIMPless Miracle: Dark-Matter Particles without Weak-Scale Masses or Weak Interactions, Phys. Rev. Lett. **101**, 231301 (2008).
[21] David E. Kaplan, Markus A. Luty, and Kathryn M. Zurek, Asymmetric dark matter, Phys. Rev. D **79**, 115016 (2009).
[22] Timothy Cohen, Daniel J. Phalen, Aaron Pierce, and Kathryn M. Zurek, Asymmetric dark matter from a GeV hidden sector, Phys. Rev. D **82**, 056001 (2010).
[23] Xiaoyong Chu, Thomas Hambye, and Michel H. G. Tytgat, The four basic ways of creating dark matter through a portal, J. Cosmol. Astropart. Phys. 05 (2012) 034.
[24] Kaustubh Agashe, Yanou Cui, Lina Necib, and Jesse Thaler, (In)direct detection of boosted dark matter, J. Cosmol. Astropart. Phys. 10 (2014) 062.
[25] Yonit Hochberg, Eric Kuflik, Tomer Volansky, and Jay G. Wacker, Mechanism for Thermal Relic Dark Matter of Strongly Interacting Massive Particles, Phys. Rev. Lett. **113**, 171301 (2014).
[26] Yonit Hochberg, Eric Kuflik, Hitoshi Murayama, Tomer Volansky, and Jay G. Wacker, Model for Thermal Relic Dark Matter of Strongly Interacting Massive Particles, Phys. Rev. Lett. **115**, 021301 (2015).
[27] Hyun Min Lee and Min-Seok Seo, Communication with SIMP dark mesons via Z' -portal, Phys. Lett. B **748**, 316 (2015).
[28] Yonit Hochberg, Eric Kuflik, and Hitoshi Murayama, SIMP spectroscopy, J. High Energy Phys. 05 (2016) 090.
[29] Eder Izaguirre, Gordan Krnjaic, Philip Schuster, and Natalia Toro, Analyzing the discovery potential for light dark matter, Phys. Rev. Lett. **115**, 251301 (2015).
[30] Nicolas Bernal and Xiaoyong Chu, $\mathbb{Z}_2$ SIMP dark matter, J. Cosmol. Astropart. Phys. 01 (2016) 006.
[31] Joachim Kopp, Jia Liu, Tracy R. Slatyer, Xiao-Ping Wang, and Wei Xue, Impeded dark matter, J. High Energy Phys. 12 (2016) 033.
[32] Soo-Min Choi, Yoo-Jin Kang, and Hyun Min Lee, On thermal production of self-interacting dark matter, J. High Energy Phys. 12 (2016) 099.
[33] Ujjal Kumar Dey, Tarak Nath Maity, and Tirtha Sankar Ray, Light dark matter through assisted annihilation, J. Cosmol. Astropart. Phys. 03 (2017) 045.
[34] Nicolás Bernal, Xiaoyong Chu, and Josef Pradler, Simply split strongly interacting massive particles, Phys. Rev. D **95**, 115023 (2017).
[35] James M. Cline, Hongwan Liu, Tracy Slatyer, and Wei Xue, Enabling forbidden dark matter, Phys. Rev. D **96**, 083521 (2017).
[36] Simon Knapen, Tongyan Lin, and Kathryn M. Zurek, Light dark matter: Models and constraints, Phys. Rev. D **96**, 115021 (2017).
[37] Miguel Escudero Abenza, Precision early universe thermodynamics made simple: $N_{\rm eff}$ and neutrino decoupling in the Standard Model and beyond, J. Cosmol. Astropart. Phys. 05 (2020) 048.
[38] Cyril Pitrou, Alain Coc, Jean-Philippe Uzan, and Elisabeth Vangioni, Precision big bang nucleosynthesis with improved Helium-4 predictions, Phys. Rep. **754**, 1 (2018).
[39] Rouven Essig, Marivi Fernandez-Serra, Jeremy Mardon, Adrian Soto, Tomer Volansky, and Tien-Tien Yu, Direct detection of sub-GeV dark matter with semiconductor targets, J. High Energy Phys. 05 (2016) 046.

[40] Eder Izaguirre, Yonatan Kahn, Gordan Krnjaic, and Matthew Moschella, Testing light dark matter coannihilation with fixed-target experiments, Phys. Rev. D **96**, 055007 (2017).

[41] Asher Berlin, Nikita Blinov, Gordan Krnjaic, Philip Schuster, and Natalia Toro, Dark matter, millicharges, axion and scalar particles, gauge bosons, and other new physics with LDMX, Phys. Rev. D **99**, 075001 (2019).

[42] Marco Battaglieri *et al.*, US Cosmic Visions: New Ideas in Dark Matter 2017: Community Report, in U.S. Cosmic Visions: New Ideas in Dark Matter (2017), arXiv:1707.04591.

[43] N. Aghanim *et al.* (Planck Collaboration), Planck 2018 results. VI. Cosmological parameters, Astron. Astrophys. **641**, A6 (2020).

[44] P. A. Zyla *et al.* (Particle Data Group), Review of Particle Physics, Prog. Theor. Exp. Phys. **2020**, 083C01 (2020).

[45] Ryan J. Cooke, Max Pettini, and Charles C. Steidel, One percent determination of the primordial deuterium abundance, Astrophys. J. **855**, 102 (2018).

[46] See Supplemental Material at http://link.aps.org/supplemental/10.1103/PhysRevLett.129.021302 for Appendices A through D, which include additional references to Refs. [47–52], contain details of the analytical and numerical calculations.

[47] Scott Dodelson, *Modern Cosmology* (Academic Press, Amsterdam, 2003).

[48] G. Fiorentini, E. Lisi, Subir Sarkar, and F. L. Villante, Quantifying uncertainties in primordial nucleosynthesis without Monte Carlo simulations, Phys. Rev. D **58**, 063506 (1998).

[49] Alexandre Arbey, Sylvain Fichet, Farvah Mahmoudi, and Grégory Moreau, The correlation matrix of Higgs rates at the LHC, J. High Energy Phys. 11 (2016) 097.

[50] Alexandre Arbey, AlterBBN: A program for calculating the BBN abundances of the elements in alternative cosmologies, Comput. Phys. Commun. **183**, 1822 (2012).

[51] A. Arbey, J. Auffinger, K. P. Hickerson, and E. S. Jenssen, AlterBBN v2: A public code for calculating Big-Bang nucleosynthesis constraints in alternative cosmologies, Comput. Phys. Commun. **248**, 106982 (2020).

[52] Hongwan Liu, Gregory W. Ridgway, and Tracy R. Slatyer, Code package for calculating modified cosmic ionization and thermal histories with dark matter and other exotic energy injections, Phys. Rev. D **101**, 023530 (2020).

[53] Cyril Pitrou, Alain Coc, Jean-Philippe Uzan, and Elisabeth Vangioni, A new tension in the cosmological model from primordial deuterium?, Mon. Not. R. Astron. Soc. **502**, 2474 (2021).

[54] V. Mossa *et al.*, The baryon density of the Universe from an improved rate of deuterium burning, Nature (London) **587**, 210 (2020).

[55] 2018 Planck Explanatory Supplement, https://wiki.cosmos.esa.int/planck-legacy-archive/index.php/Main_Page, accessed: 2021-5-14.

[56] Peter Ade *et al.* (Simons Observatory Collaboration), The Simons Observatory: Science goals and forecasts, J. Cosmol. Astropart. Phys. 02 (2019) 056.

[57] Viatcheslav F. Mukhanov, Nucleosynthesis without a computer, Int. J. Theor. Phys. **43**, 669 (2004).

[58] Tsung-Han Yeh, Keith A. Olive, and Brian D. Fields, The impact of new $d(p,\gamma)^3$He rates on Big Bang Nucleosynthesis, J. Cosmol. Astropart. Phys. 03 (2021) 046.

[59] Ofelia Pisanti, Gianpiero Mangano, Gennaro Miele, and Pierpaolo Mazzella, Primordial Deuterium after LUNA: Concordances and error budget, J. Cosmol. Astropart. Phys. 04 (2021) 020.

[60] Rouven Essig, Aaron Manalaysay, Jeremy Mardon, Peter Sorensen, and Tomer Volansky, First Direct Detection Limits on sub-GeV Dark Matter from XENON10, Phys. Rev. Lett. **109**, 021301 (2012).

[61] Rouven Essig, Tomer Volansky, and Tien-Tien Yu, New constraints and prospects for sub-GeV dark matter scattering off electrons in Xenon, Phys. Rev. D **96**, 043017 (2017).

[62] P. Agnes *et al.* (DarkSide Collaboration), Constraints on Sub-GeV Dark-Matter–Electron Scattering from the DarkSide-50 Experiment, Phys. Rev. Lett. **121**, 111303 (2018).

[63] E. Aprile *et al.* (XENON Collaboration), Light Dark Matter Search with Ionization Signals in XENON1T, Phys. Rev. Lett. **123**, 251801 (2019).

[64] L. Barak, I. M. Bloch, M. Cababie, G. Cancelo, L. Chaplinsky *et al.* (SENSEI Collaboration), SENSEI: Direct-Detection Results on sub-GeV Dark Matter from a New Skipper-CCD, Phys. Rev. Lett. **125**, 171802 (2020).

[65] Chen Cheng *et al.* (PandaX-II Collaboration), Search for Light Dark Matter-Electron Scatterings in the PandaX-II Experiment, Phys. Rev. Lett. **126**, 211803 (2021).

[66] S. Adler *et al.* (E787 Collaboration), Search for the decay $K+-->$ pi + nu anti-nu in the momentum region P(pi) less than 195-MeV/c, Phys. Lett. B **537**, 211 (2002).

[67] A. V. Artamonov *et al.* (BNL-E949 Collaboration), Study of the decay $K^+ \to \pi^+ \nu\bar{\nu}$ in the momentum region $140 < P_\pi < 199$ MeV$/c$, Phys. Rev. D **79**, 092004 (2009).

[68] Patrick deNiverville, Maxim Pospelov, and Adam Ritz, Observing a light dark matter beam with neutrino experiments, Phys. Rev. D **84**, 075020 (2011).

[69] Brian Batell, Rouven Essig, and Ze'ev Surujon, Strong Constraints on Sub-GeV Dark Sectors from SLAC Beam Dump E137, Phys. Rev. Lett. **113**, 171802 (2014).

[70] D. Banerjee, V. E. Burtsev, A. G. Chumakov, D. Cooke, P. Crivelli, E. Depero, A. V. Dermenev, S. V. Donskov, R. R. Dusaev, T. Enik *et al.*, Dark Matter Search in Missing Energy Events with NA64, Phys. Rev. Lett. **123**, 121801 (2019).

[71] J. P. Lees *et al.* (*BABAR* Collaboration), Search for Invisible Decays of a Dark Photon Produced in e^+e^- Collisions at *BABAR*, Phys. Rev. Lett. **119**, 131804 (2017).

[72] Tongyan Lin, Hai-Bo Yu, and Kathryn M. Zurek, On symmetric and asymmetric light dark matter, Phys. Rev. D **85**, 063503 (2012).

[73] Tracy R. Slatyer, Indirect dark matter signatures in the cosmic dark ages. I. Generalizing the bound on s-wave dark matter annihilation from Planck results, Phys. Rev. D **93**, 023527 (2016).

[74] Gary Steigman, Basudeb Dasgupta, and John F. Beacom, Precise relic WIMP abundance and its impact on searches for dark matter annihilation, Phys. Rev. D **86**, 023506 (2012).

[75] Jonathan L. Feng and Jordan Smolinsky, Impact of a resonance on thermal targets for invisible dark photon searches, Phys. Rev. D **96**, 095022 (2017).

[76] Manuel A. Buen-Abad, Rouven Essig, David McKeen, and Yi-Ming Zhong, Cosmological constraints on dark matter interactions with ordinary matter, Phys. Rep. **961**, 1 (2022).

[77] David Nguyen, Dimple Sarnaaik, Kimberly K. Boddy, Ethan O. Nadler, and Vera Gluscevic, Observational constraints on dark matter scattering with electrons, Phys. Rev. D **104**, 103521 (2021).

[78] Kaustubh Agashe, Steven J. Clark, Bhaskar Dutta, and Yuhsin Tsai, Nonlocal effects from boosted dark matter in indirect detection, Phys. Rev. D **103**, 083006 (2021).

[79] Fernando Perez and Brian E. Granger, IPython: A System for Interactive Scientific Computing, Comput. Sci. Eng. **9**, 21 (2007).

[80] Thomas Kluyver, Benjamin Ragan-Kelley, Fernando Pérez, Brian E. Granger, Matthias Bussonnier, Jonathan Frederic, Kyle Kelley, Jessica B. Hamrick, Jason Grout, Sylvain Corlay, Paul Ivanov, Damián Avila, Safia Abdalla, Carol Willing *et al.*, Jupyter notebooks—a publishing format for reproducible computational workflows, in *ELPUB* (IOS Press, 2016).

[81] J. D. Hunter, Matplotlib: A 2d graphics environment, Comput. Sci. Eng. **9**, 90 (2007).

[82] Stéfan van der Walt, S. Chris Colbert, and Gaël Varoquaux, The NumPy Array: A structure for efficient numerical computation, Comput. Sci. Eng. **13**, 22 (2011).

[83] Eric Jones, Travis Oliphant, Pearu Peterson *et al.*, SciPy: Open source scientific tools for Python (2001) (Online; accessed August 26, 2019).